ACS APPLIED MATERIALS & INTERFACES

Research Article

www.acsami.org

Mechanical Properties and Interface Characteristics of Nanoporous Low-*k* Materials

Lina Si,[†,‡] Dan Guo,*[,†] Guoxin Xie,*[,†] and Jianbin Luo[†]

[†]State Key Laboratory of Tribology, Tsinghua University, Beijing 100084, China

[‡]School of Mechanical Engineering, Beijing Institute of Technology, Beijing 100081, China

ABSTRACT: Low dielectric constant (low-*k*) insulator films with outstanding mechanical strength and fracture resistance are needed urgently for the new generation of ultra-large-scale integrated circuits (ULSI). In this paper, the mechanical properties of low-*k* materials and the adhesion strengths between these materials with silica have been analyzed by using molecular dynamics (MD) simulations. Atomistic models of two kinds of representative low-*k* materials [nanoporous amorphous silica (n-a-SiO_2) and SiOCH] and their contact models with silica have been constructed. The mechanical strength of the n-a-SiO_2 film decreased with the increase of porosity, and the relationship between the normalized elastic modulus and porosity was modeled. The modulus of the SiOCH film with $-CH_2-$ groups was enhanced compared with that without $-CH_2-$ groups, and the mechanism was discussed. Through investigations of the adhesion strengths between n-a-SiO_2, SiOCH, and silica, it was shown that the adhesion strengths of the n-a-SiO_2/silica interfaces decreased with porosity. The adhesion strengths of the SiOCH films with both $-CH_2-$ groups and $-CH_3$ groups were higher than that of the SiOCH film merely with $-CH_3$ groups.

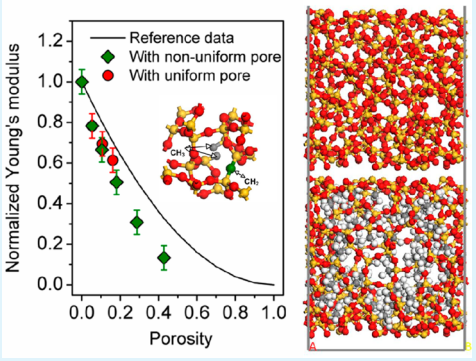

KEYWORDS: *low-k material, SiOCH film, nanoporous amorphous silica, mechanical properties, interface adhesion strength, porosities*

1. INTRODUCTION

As continuous reduction of the feature sizes in semiconductor integrated circuits (ICs), new interconnect insulator materials with low dielectric constants (low-*k*) are demanded for preventing signal delays and cross-talks.[1−3] For instance, the *k* values of low-*k* materials required for the technology nodes down to 10 nm are below 2.3, while it is 4.0 for traditional insulating materials (i.e., silica).[4,5] The low-*k* value could be achieved by lowering the polarity and the mass density of materials. For instance, the carbon-doped silica (SiOCH), a promising low-*k* material with *k* values of 2.4−3.0, has been obtained by partial replacement of Si−O bonds by less polarizable Si−C bonds.[2] Nanoporous amorphous silica (n-a-SiO_2) with many pores or gaps inside is another low-*k* material used in microelectronics.[6,7] Addition of pores or gaps to existing low-*k* materials has been commonly recognized as the only manufacturing-compatible way to get *k* values below 2.5.[4]

Nevertheless, decreasing *k* value usually results in the concomitant reduction in the mechanical strength of the low-*k* materials. The elastic modulus of the low-*k* material is typically several gigapascals, which is much lower than that of SiO_2 (70−80 GPa).[8,9] Because of their poor mechanical strength, integrating low-*k* materials successfully into the ICs is extremely difficult, especially with regard to the device packaging and chemical mechanical polishing (CMP) process.[10−12] Delamination and cracks of low-*k* films could be induced during CMP due to the large difference in the mechanical strengths of different layers[13] and lead to decreased reliability and degraded performance of IC chips. The poor ability to withstand the thermal and mechanical stresses, as well as the weak adhesion between the low-*k* material and its neighboring structure, has become the major roadblock in the effective applications of low-*k* materials.[14]

Great effort has been made in the syntheses of low-*k* materials, and the most promising low-*k* material is SiOCH, owing to the easy integration with existing semiconductor manufacturing processes.[5] Their mechanical and fracture properties have been studied by depth-sensing nanoindentation techniques.[15−18] The effect of porosity on their mechanical properties was also analyzed by Fourier transform infrared spectroscopic ellipsometry, and the results showed that the porosity of low-*k* materials strongly affected their mechanical properties.[15] Extensive experiments have been done to seek ways to improve the elastic modulus and the fracture toughness of SiOCH thin films.[19,20] It was demonstrated that the elastic modulus of SiOCH films could be improved by thermal treatment and ultraviolet irradiation, through which part of the terminal groups (e.g., −OH and $-CH_3$) was lost and the degree of cross-linking of networking bonds was increased.[19] On the basis of the same principle, Dubois et al.[20] obtained SiOCH films with remarkable mechanical properties by adopting precursor monomers, in which hydrocarbon molecules (e.g., $-CH_2-CH_2-$) were contained and could be incorporated into the material matrix as network-forming units,

Received: May 26, 2014
Accepted: August 5, 2014
Published: August 5, 2014

resulting in a less disrupted network with improved mechanical strengths. Furthermore, the mechanical properties of low-*k* material obtained by plasma-enhanced chemical vapor deposition (PECVD) are affected by the porogen residues. Urbanowicz et al.[16,21−23] proposed an approach to fabricate porogen-residue-free PECVD SiOCH films with improved mechanical properties and ultralow-*k* values by selective porogen removal prior to an ultraviolet-assisted hardening step, and the mechanisms for the improvement of mechanical properties were interpreted by the continuous random network theory and percolation of rigidity concepts.[24−26] It indicated that the mechanical properties of SiOCH films significantly depended on the ratio of D (Si with two O atoms and two terminal groups) to T (Si with three O atoms and one terminal group).

In addition to the experimental studies on the mechanical properties of low-*k* materials, theoretical modeling is also indispensable for understanding the underlying mechanisms. Finite element method (FEM) could provide insightful analyses to the dielectric reliability. The degradation processes, due to electromigration and stress-induced voiding, were investigated by using the FEM method, and the potential failure sites were identified.[27] Moreover, the FEM method could be used to examine the origin of the mechanical cracking of dielectrics during the CMP process by analyzing the stress distribution of Cu/low-*k* interconnect structures.[28,29] The first-principle calculations (such as density functional theory, DFT) generally focused on the investigations of the structural features of low-*k* materials,[30] and it could be also used to investigate the adsorption properties of porous materials[31] and the interaction of the interfaces between different materials.[31,32] Molecular dynamics (MD) methods have been used to construct the atomistic models of low-*k* materials with different compositions, and the mechanical stiffness as well as the fracture toughness properties were analyzed.[14,33−38] Methods creating the molecular models of SiOCH films were developed by Tajima et al.,[34,35] Yuan et al.,[36,37] Li et al.,[38] and Knaup et al.,[39] and reasonable SiOCH film structures could be generated with these methods for the investigations of the Young's modulus and the dielectric constant. Dubois et al. obtained SiOCH films with a less disrupted network by using precursor bridging monomer structures. It was found that, compared with the common SiOCH films with identical *k* values, the mechanical stiffness of the SiOCH films with a less disruptive network was enhanced obviously.[40] However, owing to the complexity of the amorphous dielectrics, the computational studies of the low-*k* materials are still in their infancy.

In this paper, atomistic models of two kinds of low-*k* materials were established. In order to investigate the influence of porosities on the mechanical properties and its interface adhesion with its neighboring structure, nanoporous amorphous silica with varied porosities was constructed. On the basis of the nanoporous amorphous silica constructed previously, two classes of SiOCH models were established to elucidate the respective roles of bridging and terminal groups. Here the bridging and terminal groups we focused on were $-CH_2-$ and $-CH_3$, respectively, because they are the simplest and only one carbon included. The first class of the SiOCH models have only Si−O−Si bonds in the network, and amount of $-CH_3$ groups are included. The second class of the SiOCH models consist of both Si−O−Si and Si−CH_2−Si bonds in the network, and amount of $-CH_3$ terminal groups. The mechanical properties of these low-*k* materials, as well as the interfacial adhesion strengths between these materials and silica, have been investigated. Emphases were put on the relationships between the mechanical stiffness as well as the interfacial adhesion strength and the porosity of low-*k* materials as well as the introduction of $-CH_2-$ groups.

2. ATOMISTIC MODELING AND SIMULATION METHODS

2.1. Models of Two Kinds of Low-*k* Materials. *2.1.1. Nanoporous Amorphous Silica (n-a-SiO_2).* Nanoporous amorphous silica with closed pores has been constructed according to Li's method.[38] The construction steps of n-a-SiO_2 are as follows: first, a silicon crystal with the diamond cubic structure was melted and quenched to obtain the amorphous silicon. Subsequently, the crystal lattice of the amorphous silicon was elongated 1.338 times in all the three dimensions. After expansion, the Si−O−Si bond with an angle of 150° was used to replace the Si−Si bond with a random orientation. By using this method, an amorphous silica model with a mass density of 2.2 g/cm^3 was created, and the model was relaxed by potential energy minimization. The simulation strategy for the relaxation will be provided in details below.

In order to obtain n-a-SiO_2 with various porosities, pores with different diameters were created in the amorphous silica model by removing silicon and oxygen atoms in the pores. The amount of the removed atoms was determined as follows: taking the generation of 1 nm pore for an example, first the silicon and oxygen atoms in a spherical ball with a diameter of 1 nm were selected from the amorphous silica model, and the number of the selected atoms was counted. Since the choice of the spherical ball center could influence the number of the atoms inside, the number of silicon and oxygen atoms inside the spherical ball with a defined diameter was the average of 10 groups, in which the center of the spherical ball was randomly selected. A function describing the relationship between the number of silicon and oxygen atoms (y) and the diameter of the amorphous silica ball (x) can be obtained: $y = ax^3$; the coefficient a is 40. For example, the number of atoms which should be removed to get a pore with a diameter of 1 nm in the amorphous silica model is 40.

The pore sizes in the low-*k* materials used in engineering are usually in the range of 1−2 nm. Hence, five groups of n-a-SiO_2 structures were generated with pore diameters of 1, 1.25, 1.5, 1.75, and 2.0 nm, referred to as n-a-SiO_2 model 1 to n-a-SiO_2 model 5, respectively. However, these models had nonuniform pore sizes. In order to separate the porosity effect from the pore size effect on the mechanical properties of n-a-SiO_2, another two groups of n-a-SiO_2 structures with different porosities were constructed by creating two or three pores with a uniform pore diameter of 1 nm, referred to as n-a-SiO_2 model 6 and n-a-SiO_2 model 7, respectively. Ideally, the pores are expected to be all aligned and equally distributed in the simulation cell; however, it is difficult to achieve. In order to lessen the impact of pore distribution, we generate each group (n-a-SiO_2 model 6 or 7) with 50 guesses. And the mass densities and moduli are obtained by calculating the averages of 50 guesses in each group. In this article, porosity p was defined as the fraction of the volume occupied by pores: $p = V_P/V_T$, where V_P was the pore volume and V_T the total volume of the n-a-SiO_2 model. The detailed structural parameters of the above amorphous silica and n-a-SiO_2 models are summarized in Table 1.

The schematic models of the constructed amorphous silica and n-a-SiO_2 are shown in Figure 1, in which the yellow and red balls represent the silicon and oxygen atoms, respectively. In the initial amorphous silica and n-a-SiO_2 models, the ratio of oxygen to silicon atoms was 2:1, and the lattice parameters of the cubic crystal were $a = b = c =$ 21.3949 Å, $\alpha = \beta = \gamma = 90°$. Preliminary simulations of the n-a-SiO_2 models, which were 8 times larger in the cell size than the models presented in this paper, suggested that the finite size effect was insignificant for the properties investigated in this work. The length of Si−O bond was approximately 1.61 Å, and the Si−O−Si angle 148° in the models. With the increase of porosity, the number of the atoms included in the n-a-SiO_2 models decreased. For instance, n-a-SiO_2 model 5 with a spherical pore of 2 nm in diameter included 328 atoms, and its porosity was 42.77%. It can be seen from Figure 1 that the

Table 1. Structural Parameters of Amorphous Silica and n-a-SiO_2 Models

models	lattice size	pore diameter (nm)	pore no.	atom no.	porosity (%)
amorphous silica	$a = b = c =$ 21.3949 Å	0	0	648	0
n-a-SiO_2 model 1		1	1	608	5.35
n-a-SiO_2 model 2		1.25	1	570	10.44
n-a-SiO_2 model 3		1.5	1	513	18.04
n-a-SiO_2 model 4		1.75	1	434	28.65
n-a-SiO_2 model 5		2	1	328	42.77
n-a-SiO_2 model 6		1	2	568	10.70
n-a-SiO_2 model 7		1	3	528	16.05

structures with lower porosity are denser than those with the higher porosity.

2.1.2. SiOCH Films. SiOCH films which are composed of a Si−O base with the incorporation of $-CH_3$ groups have been widely studied as a promising candidate for interlayer dielectric applications. Typical densities of SiOCH films are between 1.2 and 1.4 g/cm^3; k value are close to 2.4−3, and it can go to less than 2.3.[2] In this work, theoretical models of SiOCH films were constructed. The SiOCH film possessed similar network structure of Si−O bonds to the silica film. The difference was that part of the oxygen atoms in the silica film was replaced by $-CH_3$, −H, or −OH groups, and the initial network structure was broken down.[36,38,40]

On the basis of the n-a-SiO_2 model 3 constructed previously, two groups of SiOCH models were obtained. For one group of the SiOCH models (referred to as SiOCH model 1), 16.67% of the bridging oxygen atoms in the backbone structure of n-a-SiO_2 model 3 were broken and the oxygen atoms were replaced by two $-CH_3$ groups (as shown in Figure 2, parts a and b, the oxygen atom A). The ratio of Si to $-CH_3$ was 1:0.67. For the other group of the SiOCH models (referred to as SiOCH model 2), 14.17% of the bridging oxygen atoms were converted into pairs of Si−CH_3 units, and 5% of the bridging oxygen atoms were replaced by $-CH_2-$ groups (as shown in Figure 2, parts a and b, the oxygen atom B). The ratio of Si:$-CH_2-$:$-CH_3$ was 1:0.1:0.57. The main structural parameters of the SiOCH models are given in Table 2, and the SiOCH models are schematically shown in Figure 2, parts c and d. For statistical purposes, 10 configurations, in which terminal positions were randomly selected, were constructed for each composition.

2.1.3. Interfacial Models of Low-k Materials and Silica. The interfacial models for low-k/silica were established to investigate the interfacial strength at the interface. Taking the interfacial model for n-a-SiO_2/silica as an example, the construction steps were as follows: first, the surface model of amorphous silica was established with a dimension of 21.3949 Å × 21.3949 Å × 21.3949 Å along the x-, y-, and z-directions. Subsequently, the surface models of n-a-SiO_2 were constructed with a dimension of 21.3949 Å × 21.3949 Å × 21.3949 Å along the x-, y-, and z-directions. On the basis of these surface models, interfacial models for n-a-SiO_2/silica were constructed, and the interfacial model for n-a-SiO_2 model 3/silica is schematically shown in Figure 3a. Similarly, the interfacial models for SiOCH model 1/silica (Figure 3b) and SiOCH model 2/silica were constructed.

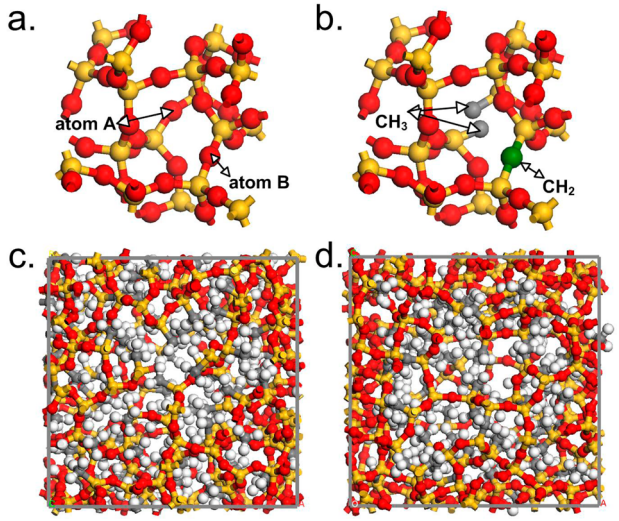

Figure 2. (a) Broken view of the backbone structure of n-a-SiO_2. (b) Illustration in which the oxygen atom A replaced by two $-CH_3$ groups and the oxygen atom B replaced by $-CH_2-$ groups. (c) SiOCH model 1. (d) SiOCH model 2. Yellow, red, gray, and white balls represent silicon, oxygen, carbon, and hydrogen atoms, respectively.

2.2. Simulation Method. MD simulation was conducted using the software package of Material Studio and the COMPASS force field which has been extensively used to simulate a-SiO_2, n-a-SiO_2, and SiOCH systems.[41] The comparison between the obtained results with the accurate DFT calculations and experimental data proved that such a force field could correctly predict the mechanical properties of these systems.[14,38]

In the COMPASS force field, the total energy of a system can be expressed as a sum of valence interactions, valence cross-terms, and nonbond interactions including the van der Waals and electrostatic terms. The cutoff distance for the calculation of van der Waals interaction was set to 9.5 Å with long-range correction considered. Ewald summation method with a cutoff distance of 12.5 Å was used for the electrostatic interaction. Periodic boundary conditions were employed in the MD simulations. The equations of the motion of atoms were solved using the velocity Verlet method, and the time step used was 1 fs.

In order to obtain the equilibrium states of the system, the sample was first optimized with NVT dynamics for 10 ps maintaining the temperature and the volume constant. Then NPT dynamics with constant pressure and temperature were carried out for more than 100 ps depending on the model investigated to guarantee the energy of the system to reach the steady state. The temperature was controlled by the Andersen method and the pressure by the Parrinello method. After

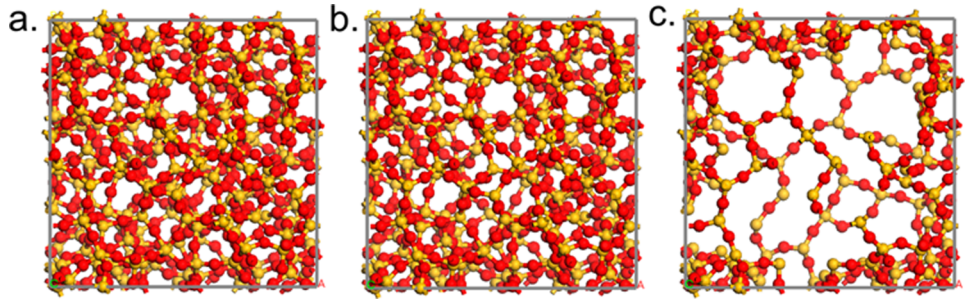

Figure 1. Schematic models of the constructed amorphous silica and n-a-SiO_2: (a) amorphous silica model without pores; (b) n-a-SiO_2 model 1 with one pore of 1 nm; (c) n-a-SiO_2 model 5 with one pore of 2 nm. Yellow balls represent silicon atoms, and red ones represent oxygen atoms.

Table 2. Main Structural Parameters of the SiOCH Models

models	lattice size	pore diameter (nm)	porosity (%)	atom ratio of Si:O:CH_2:CH_3
SiOCH model 1	$a = b = c = 21.3949$ Å	1.5	18.04	1:1.66:0:0.67
SiOCH model 2	$a = b = c = 21.3949$ Å	1.5	18.04	1:1.62:0.1:0.57

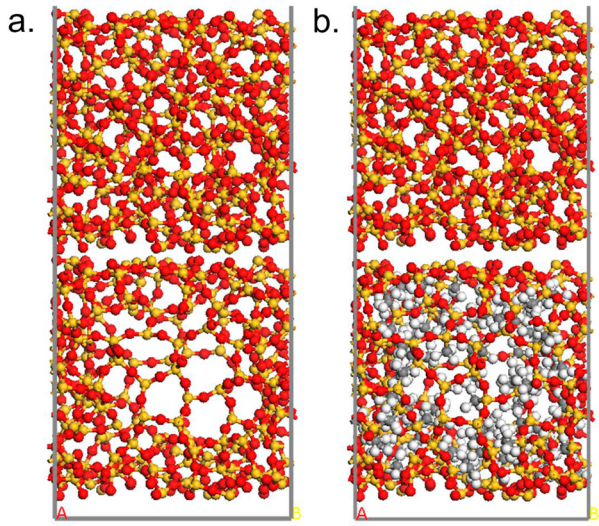

Figure 3. (a) Interfacial model of n-a-SiO_2 model 3/silica. (b) Interfacial model of SiOCH model 1/silica. Yellow, red, gray, and white balls represent silicon, oxygen, carbon, and hydrogen atoms, respectively.

equilibration, NPT dynamics was continued for another 20 ps to generate trajectories for properties sampling, such as mechanical properties and interfacial interaction energies. To obtain the mechanical properties, three tensile and three pure shear deformations were applied to the minimized undeformed system and the system was reminimized following each deformation. The internal stress tensor was then obtained from the analytically calculated virial and used to obtain the estimates of the six columns of the elastic stiffness coefficients matrix. The bulk modulus and shear modulus were calculated from the elastic constants.[38]

In this work, the interfacial adhesion interaction (E_{int}) between low-k films and silica was calculated by using the following equation:[42,43]

$$E_{int} = E_{tot} - (E_{low\text{-}k} + E_{silica}) \quad (1)$$

where E_{tot} is the total internal energy of the low-k films/silica system, $E_{low\text{-}k}$ is the energy of the individual low-k film, and E_{silica} is the energy of silica. In the Accelrys MD software, the unit of interaction energy is kcal/mol, where "mol" means a mole number of system molecules in the periodic condition. Therefore, the area of the interface is a mole number of interface in a single system with a thickness of 10.697 Å and the unit of the interaction energy becomes Joules per square meter (J/m^2). Therefore, the following equation is used to calculate the interaction energy in our simulations:

$$E_{int\_area} = [E_{tot} - (E_{low\text{-}k} + E_{silica})]/surface\_area \quad (2)$$

If the interaction energy is negative, there is an attractive force between the objects, such as adhesion; if it is positive, there is a repulsive force.

3. RESULTS AND DISCUSSION

3.1. Mechanical Properties of the Low-k Films.

3.1.1. Mechanical Properties of n-a-SiO_2 Films. Prior to calculating the mechanical properties of n-a-SiO_2 films, the system should reach the equilibrium state, and hence relaxation processes to the n-a-SiO_2 films were carried out. During the geometry optimization process, atomic coordinates and lattice parameters were optimized simultaneously. The structures after the relaxation process are shown in Figure 4. The lattice shapes of the amorphous silica without pores (Figure 4a) and the n-a-SiO_2 with relatively smaller porosities, such as n-a-SiO_2 model 1 (Figure 4b), did not change obviously, e.g., the lattice parameters of n-a-SiO_2 model 1 after relaxation were a = 20.99 Å, b = 21.08 Å, c = 21.26 Å, α = 90.41°, β = 90.03°, γ = 89.75°. In contrast, more obvious changes of the lattice shapes can be observed for those films with relatively larger porosities, e.g., the lattice parameters of n-a-SiO_2 model 5 (Figure 4c) after relaxation were a = 21.07 Å, b = 21.58 Å, c = 20.81 Å, α = 90.57°, β = 86.30°, γ = 94.36°.

After the system reached the equilibrium, typical properties of the n-a-SiO_2 films were investigated. The calculated mass density of amorphous silica was 2.32 g/cm^3, being very close to the experimentally measured value of 2.2 g/cm^3.[44] The calculated elastic modulus (the average of the elastic moduli in three directions) of amorphous silica was 88.73 GPa, which slightly deviated from the experimentally measured value of about 76 GPa.[45,46] One reasonable explanation of this trend was that the material in MD simulations represented a nearly perfect molecular structure, while the samples in experiments usually contained macroscopic or large microscopic defects, and therefore the calculated values could be considered as the upper limit of the referenced ones.[47,48]

Figure 5a shows the relationship between the calculated densities and the porosities of the n-a-SiO_2 models. It can be

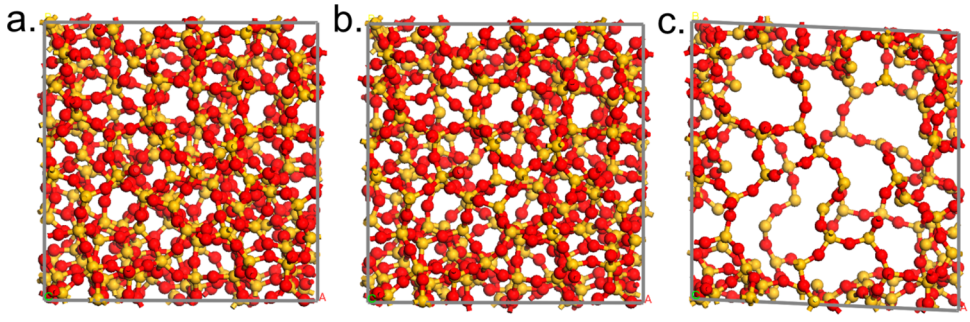

Figure 4. Schematic models of n-a-SiO_2 after relaxation : (a) amorphous silica model without pore; (b) n-a-SiO_2 model 1; (c) n-a-SiO_2 model 5. Yellow balls represent silicon atoms, and red ones represent oxygen atoms.

dx.doi.org/10.1021/am503236m | ACS Appl. Mater. Interfaces 2014, 6, 13850−13858

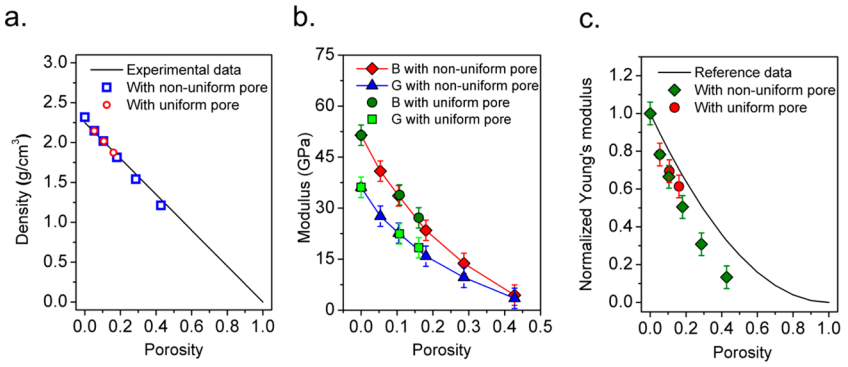

Figure 5. (a) Relationship between the calculated densities and porosities of n-a-SiO_2 films, and a line fitted with experimentally measured values is also plotted for reference (ref 45). (b) Various curves of the calculated moduli to porosity; B and G represent bulk modulus and shear modulus. (c) The comparison between the calculated values of the normalized Young's moduli and those from experimental reference.

seen that the mass density of the n-a-SiO_2 film decreases linearly as porosity increases. The densities of nanoporous silica based films deposited by the spin on deposition (SOD) and the PECVD methods were investigated by Fisher et al.,[49] and the line fitted with experimentally measured values is plotted in Figure 5a for reference. The nanoporous silica films investigated by Fisher et al. were porous silica with evenly distributed pores of the identical diameter. As shown, our simulation results with the uniform pore sizes are in good agreement with the experimental values obtained by Fisher et al. Meanwhile, the simulation results with nonuniform pore sizes are close to the experimental data. For example, the calculated mass density of the n-a-SiO_2 model 3 is 1.813 g/cm^3 with the porosity of 18.04% based on the present model, while the measured value by Fisher is 1.844 g/cm^3, which is only 1.71% larger than the calculated value. Therefore, the density of the n-a-SiO_2 film was determined primarily by porosity, and affected slightly by the pore size in the film.

Since the calculation of the k value is quite time-consuming for a relatively large system, the k value of n-a-SiO_2 films was not calculated in this work. In the work conducted by Fisher et al., the dielectric constant of n-a-SiO_2 could be predicted by using the Lorentz−Lorenz, Rayleigh, Parallel model, and Clausius−Mossotti equation.[50,51] Therefore, the k values of the n-a-SiO_2 models were inferred from aforementioned models. For instance, according to the Parallel model, the k value of n-a-SiO_2 model 1 with a porosity of 5.35% was 3.85 and that of n-a-SiO_2 model 5 with a porosity of 42.77% was 2.7−2.8.

Next, the effects of porosity and pore size on the mechanical properties of n-a-SiO_2 films were investigated. Figure 5b and Table 3 show the relationships between the bulk modulus, shear modulus, and porosity. It can be seen that with the increase of porosity, all of the moduli decrease. The Young's moduli of the n-a-SiO_2 films with evenly distributed pore but different porosities could be obtained by the following relationship:[51]

$$E/E_b = (1 - P)^2 \quad (3)$$

where E and P are the Young's modulus and the porosity of the n-a-SiO_2 films, E_b is the Young's modulus of the amorphous silica without pores, and E/E_b is defined as the normalized Young's modulus. In Figure 5c, the normalized Young's moduli calculated in this work have been compared with the results obtained by Miyoshi et al.,[51] who investigated porous silica with evenly distributed identical pores based on the FEM method. It was shown that the normalized Young's moduli of the models with uniform pore sizes were close to the FEM calculation data, while those of models with nonuniform pore sizes were much lower than the referenced ones. It could be inferred that, with the same porosity, the normalized Young's moduli of n-a-SiO_2 films with larger pore sizes were lower than those with smaller pore sizes.

From the analyses above, it could be concluded that the mass density and the Young's modulus were influenced by the porosity of n-a-SiO_2 films dramatically. Moreover, the mechanical properties of n-a-SiO_2 films were also affected by the pore size. Evenly distributed pores with identical and smaller sizes were more beneficial for obtaining porous silica films with high performance.

3.1.2. Mechanical Properties of SiOCH Films. In the first place, relaxation processes of the SiOCH models were carried out to guarantee the system reaching an equilibrium state. Then, the mechanical properties of SiOCH models were examined, and the results are summarized in Table 4. Compared with n-a-SiO_2 model 3 from which the SiOCH models were derived in this work, both the mass densities and the mechanical stiffness of the SiOCH models reduced. Figure 6 shows the distributions of the bond length and angle in the SiOCH models, amorphous silica without pores, and n-a-SiO_2 model 3, based on which the structures of different low-k materials could be analyzed. The lengths of the Si−O bond in amorphous silica without pores and n-a-SiO_2 model 3 are both about 1.61 Å, and those in SiOCH models 1 and 2 are slightly larger. The bond angle of Si−O−Si bonds decreased slightly for SiOCH models. The decreases of the mass density and mechanical stiffness of the SiOCH model are mainly attributed to the introduction of the terminal groups ($-CH_3$) which not

Table 3. Mechanical Properties of Amorphous Silica and n-a-SiO_2 Models

models	bulk modulus (GPa)	shear modulus (GPa)	elastic modulus (GPa)
amorphous silica	51.45	36.14	88.73
n-a-SiO_2 model 1	40.88	27.63	69.43
n-a-SiO_2 model 2	33.62	22.64	58.98
n-a-SiO_2 model 3	23.48	15.86	44.82
n-a-SiO_2 model 4	13.76	9.63	27.30
n-a-SiO_2 model 5	4.43	3.49	11.83
n-a-SiO_2 model 6	33.88	22.46	61.62
n-a-SiO_2 model 7	27.15	18.34	54.45

Table 4. Mass Densities and Mechanical Properties of SiOCH Models

models	porosity (%)	density (g/cm^3)	bulk modulus (GPa)	shear modulus (GPa)	Young's modulus (GPa)
n-a-SiO_2 model 3	18.04	1.8131	25.0866	16.5567	44.8392
SiOCH model 1	18.04	1.6639	15.5017	11.6943	28.0607
SiOCH model 2	18.04	1.7383	17.5171	11.9106	30.2693

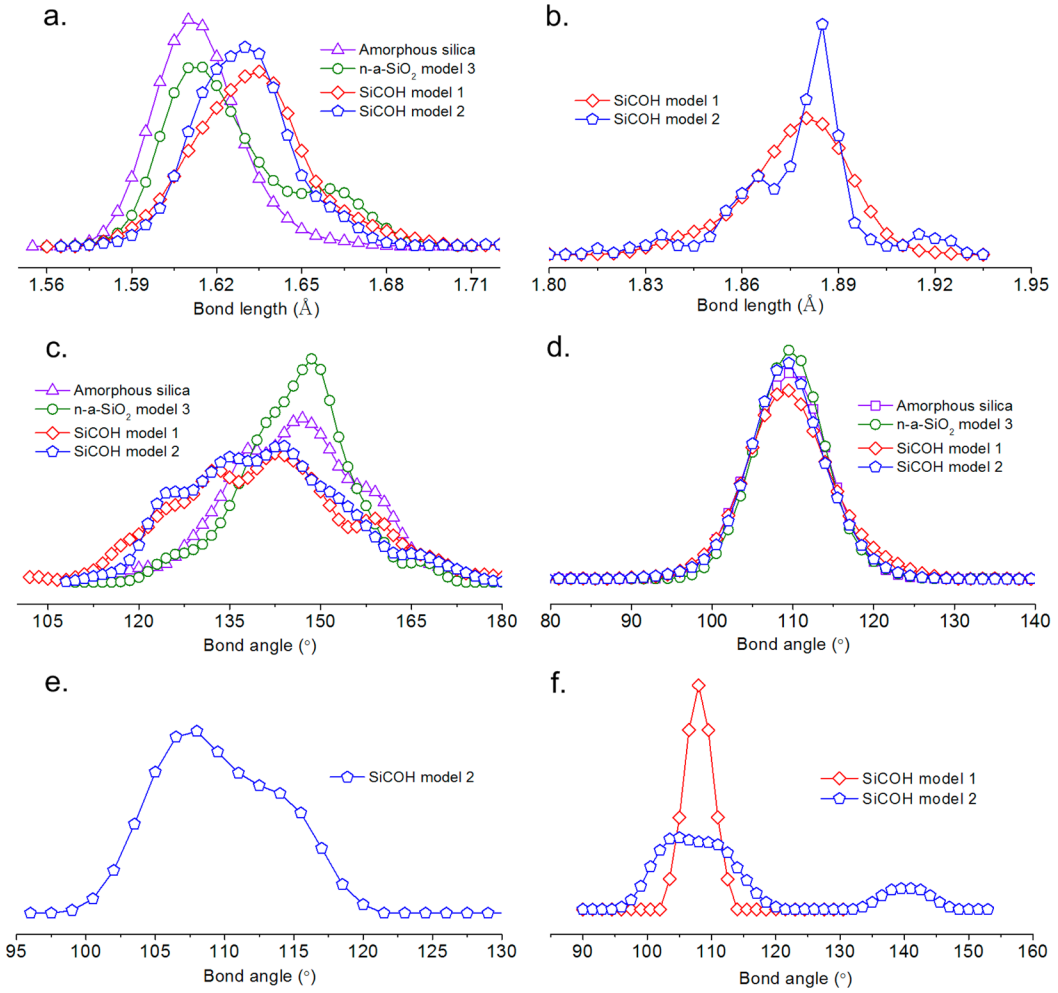

Figure 6. Distributions of bond lengths and angles in the SiOCH models, amorphous silica without pores, and n-a-SiO_2 model 3: (a) Si−O bond length distribution; (b) Si−C bond length distribution; (c) Si−O−Si bond angle distribution; (d) O−Si−O bond angle distribution; (e) Si−C−Si bond angle distribution; (f) C−Si−C bond angle distribution.

only disrupt the network of porous silica but also expand the network of SiOCH films (larger bond length of Si−C: 1.89 Å).

As shown in Table 4, both the mass densities and Young's modulus of SiOCH model 2 with both $-CH_3$ and $-CH_2-$ groups are larger than those of SiOCH model 1 in which only $-CH_3$ groups are included. As shown in Figure 6, the lengths of the Si−O bond in SiOCH model 1 are slightly larger than those in SiOCH model 2 (Figure 6a). The length of the Si−C bond in SiOCH model 1 is mainly around 1.89 Å. Two peaks of the Si−C length distribution in SiOCH model 2 exist: one peak value of 1.89 Å is the bond length of Si−CH_3, and the other peak of 1.865 Å is the bond length of Si−CH_2- (Figure 6b). And there are no obvious differences between SiOCH model 1 and SiOCH model 2 in the bond angle distributions of Si−O−Si, O−Si−O, and C−Si−C bonds (Figure 6c−f). The relatively smaller bond lengths of Si−O and Si−CH_2- bonds lead to a denser network of SiOCH model 2, thus increasing its mass density and Young's modulus. Although $-CH_2-$ group is slightly lighter than $-CH_3$ group, the denser network resulted from the reductions of Si−O and Si−CH_2- bond lengths have a dominant effect, resulting in the increase of the mass density of SiOCH model 2.

The network connectivity number can also be used to quantify the network connectivity, which is defined as the average coordination number per network-forming atom.[38] The larger the connectivity number, the denser the network structure with improved mechanical properties. The connectivity number of SiOCH model 1 can be calculated through the following equation:[38]

$$\langle r \rangle = \frac{r_{Si}N_{Si} + r_{O}N_{O} + r_{CH_3}N_{CH_3}}{N_{Si} + N_{O} + N_{CH_3}} \quad (4)$$

where N_{Si,O,CH_3} is the number of silicon atoms, bridging oxygen atoms, or $-CH_3$ groups as denoted by the subscript, and

dx.doi.org/10.1021/am503236m | ACS Appl. Mater. Interfaces 2014, 6, 13850−13858

r_{Si,O,CH_3} is the respective coordination number. The connectivity number of SiOCH model 2 can be calculated by

$$\langle r \rangle = \frac{r_{Si}N_{Si} + r_{O}N_{O} + r_{CH_2}N_{CH_2} + r_{CH_3}N_{CH_3}}{N_{Si} + N_{O} + N_{CH_2} + N_{CH_3}} \quad (5)$$

where N_{CH_2} is the number of $-CH_2-$ groups and r_{CH_2} is its coordination number. The connectivity numbers of SiOCH model 1 and 2 are 2.4 and 2.345, respectively, which are both less than that for a-silica ($\langle r \rangle$ = 2.67). The decrease of the connectivity number could be mainly attributed to the amount of terminal groups (i.e., $-CH_3$). A comparison between SiOCH model 1 and SiOCH model 2 suggests that replacing 5% oxygen bridging atoms by $-CH_2-$ bridging links instead of $-CH_3$ groups could result in a slight increase of the connectivity number. The above analyses are in agreement with the bond length and angle distribution analysis.

3.2. Interfacial Adhesion Strength between Low-*k* Materials and Silica. Geometry optimization of the simulated system has been done. During the geometry optimization process, the atoms at the interface experienced two forms of relaxation movement:[52] one was the movement along the direction perpendicular to the interface, and the other was the movement parallel to the interface. In this work, the relaxation movement perpendicular to the interface predominated in the relaxation process and no horizontal displacement occurred. The interfacial models of low-*k* materials/silica after optimization are given in Figure 7. It can be seen from Figures 3 and 7 that the initial distance between the surfaces of n-a-SiO_2 model 3 with a pore diameter of 1.5 nm and silica is larger than that after relaxation. The equilibrium distances at the interfaces of n-a-SiO_2 models/silica are around 2 Å and are not obviously affected by the sizes of pores introduced in the n-a-SiO_2 models.

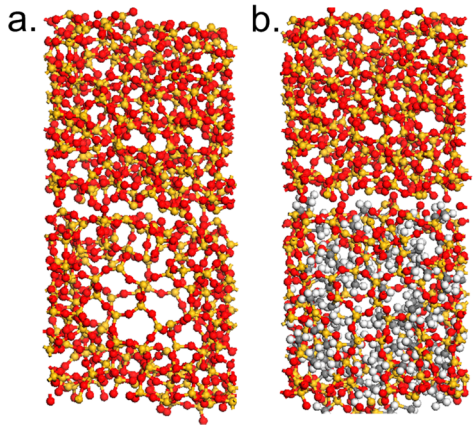

Figure 7. Interfacial models of low-*k* materials/silica after optimization: (a) n-a-SiO_2 model 3/silica interface; (b) SiOCH model 1/silica interface.

Next, the interfacial adhesions between the n-a-SiO_2 films and silica at the temperature of 298 K were calculated, and the results are summarized in Table 5. It can be seen that the absolute values of the total internal energy of the system (E_{tot}) and the energy of n-a-SiO_2 ($E_{n\text{-}a\text{-}SiO_2}$) decrease with porosity while the energy of silica (E_{SiO_2}) is almost unchanged. It can be seen that the introduction of pores into the amorphous silica lowers $E_{int\text{-}area}$ between n-a-SiO_2 films and silica. $E_{int\text{-}area}$ decreases with the increasing porosity.

Furthermore, the interfacial adhesions between SiOCH film models and silica at 298 K are given in Table 6 As shown, the adhesion interaction energies of the SiOCH model/silica interfaces are smaller than those of the n-a-SiO_2 models/silica interfaces, and the SiOCH models with $-CH_2-$ groups have a superior adhesion strength with silica than the SiOCH film models merely with $-CH_3$ groups. The introduction of $-CH_2-$ groups in the SiOCH structure not only enhances the mechanical stiffness of the film but also improves the adhesion strength between the SiOCH film and silica. Previous studies on low-*k* films revealed a linear relationship between dielectric constant or film mass density and the cohesive strength.[19] Compared with SiOCH model 1 (without $-CH_2-$ groups), SiOCH model 2 (with $-CH_2-$ groups) has a relatively larger mass density; therefore, the interfacial adhesion strength between the SiOCH model 2 and silica is relatively larger. The interfacial strength between low-*k* (SiOCH film) and silica was also investigated by Yuan et al. using molecular dynamics simulation method, and a recommendation of improving the interfacial strength was proposed based on their simulation results.[37] It was suggested that the improvement of the stiffness of low-*k* films can efficiently enhance the interfacial strength, which responds to our simulation results.

4. CONCLUSION

MD models of n-a-SiO_2 with different porosities and SiOCH films have been established, and their mechanical properties as well as the interfacial adhesion strength with silica have been analyzed. The bulk, shear, and elastic moduli of n-a-SiO_2 decreased with the porosity, and the relationship between the normalized elastic modulus and porosity was modeled, which was in good agreement with that obtained from FEM calculation results in literatures. By comparing two groups of SiOCH models, it was found that the introduction of $-CH_2-$ groups enhanced the mechanical properties of the SiOCH film, since the SiOCH film with $-CH_2-$ groups had a denser

Table 5. Relevant Energies at n-a-SiO_2 Models/Silica Interfaces

interfacial models	E_{tot} (kcal/mol)	$E_{n\text{-}a\text{-}SiO_2}$ (kcal/mol)	E_{silica} (kcal/mol)	E_{int} (kcal/mol)	$E_{int\text{-}area}$ (J/m^2)
amorphous silica/silica interface	−55444.9	−27529.4	−27575.8	−339.88	−0.537
n-a-SiO_2 model 1/silica interface	−52377.7	−27529.4	−24530.6	−317.78	−0.499
n-a-SiO_2 model 2/silica interface	−43942.6	−27529.4	−16108.9	−304.40	−0.490
n-a-SiO_2 model 3/silica interface	−39751.6	−27529.4	−16108.9	−275.57	−0.436
n-a-SiO_2 model 4/silica interface	−34290.1	−27529.4	−11946.7	−243.51	−0.384
n-a-SiO_2 model 5/silica interface	−29708.8	−27529.4	−6517.19	−206.65	−0.328
n-a-SiO_2 model 6/silica interface	−44079.6	−27529.4	−1972.76	−306.52	−0.484
n-a-SiO_2 model 7/silica interface	−38670.6	−27529.4	−16243.7	−287.33	−0.462

Table 6. Relevant Energies at the SiOCH/Silica Interfaces

interfacial models	E_{tot} (kcal/mol)	$E_{low\text{-}k}$ (kcal/mol)	E_{silica} (kcal/mol)	E_{int} (kcal/mol)	$E_{int\text{-}area}$ (J/m^2)
n-a-SiO_2 model 3/silica interface	−39751.6	−27529.4	−16108.9	−275.57	−0.436
SiOCH model 1/silica interface	−37868.4	−27529.4	−10102.3	−266.67	−0.413
SiOCH model 2/silica interface	−37702.8	−27529.4	−9945.6	−227.83	−0.352

structure than that merely with $-CH_3$ groups. Through the investigation of the interfacial adhesion strength between the n-a-SiO_2, SiOCH films, and silica, the adhesion strength of the n-a-SiO_2/silica interface was found to decrease with porosity and the introduction of $-CH_2-$ groups in SiOCH enhanced the adhesion strength.

AUTHOR INFORMATION

Corresponding Authors

*E-mail: guodan26@mail.tsinghua.edu.cn.

*E-mail: xie-gx@163.com.

Notes

The authors declare no competing financial interest.

ACKNOWLEDGMENTS

This project is supported by the National Natural Science Foundation of China (Grant Nos. 51305029 and 51375255), the China Postdoctoral Science Foundation (Nos. 2012M520005 and 2013T60066), and the Tribology Science Fund of State Key Laboratory of Tribology (SKLTKF12A03).

REFERENCES

(1) Grill, A.; Edelstein, D.; Lane, M.; Patel, V.; Gates, S.; Restaino, D.; Molis, S. Interface Engineering for High Interfacial Strength between SiCOH and Porous SiCOH Interconnect Dielectrics and Diffusion Caps. *J. Appl. Phys.* **2008**, *103*, 054104.

(2) Maex, K.; Baklano, M. R.; Shamiryan, D.; Lacopi, F.; Brongersma, S. H.; Yanovitskaya, Z. S. Low Dielectric Constant Materials for Microelectronics. *J. Appl. Phys.* **2003**, *93*, 8793.

(3) Grill, A.; Patel, V. The Effect of Plasma Chemistry on the Damage Induced to Porous SiCOH Dielectrics. *J. Electrochem. Soc.* **2006**, *153*, F169−F175.

(4) Volksen, W.; Miller, R. D.; Dubois, G. Low Dielectric Constant Materials. *Chem. Rev.* **2010**, *110*, 56−110.

(5) Baklanov, M. R.; de Marneffe, J. F.; Shamiryan, D.; Urbanowicz, A. M.; Shi, H.; Rakhimova, T. V.; Huang, H.; Ho, P. S. Plasma Processing of Low-k Dielectrics. *J. Appl. Phys.* **2013**, *113* (4), 041101.

(6) Xiao, X.; Hata, N.; Yamada, K.; Kikkawa, T. Mechanical Properties of Periodic Porous Silica Low-k Films Determined by the Twin-transducer Surface Acoustic Wave Technique. *Rev. Sci. Instrum.* **2003**, *74*, 4539.

(7) Li, H.; Tsui, T. Y.; Vlassak, J. J. Water Diffusion and Fracture Behavior in Nanoporous Low-k Dielectric Film Stacks. *J. Appl. Phys.* **2009**, *106*, 033503.

(8) Lin, Y.; Xiang, Y.; Tsui, T. Y.; Vlassak, J. J. PECVD Low-Permittivity Organosilicate Glass Coatings: Adhesion, Fracture and Mechanical Properties. *Acta Mater.* **2008**, *56*, 4932−4943.

(9) Bailey, S.; Mays, E.; Michalak, D. J.; Chebiam, R.; King, S.; Sooryakumar, R. Mechanical Properties of High Porosity Low-k Dielectric Nano-films Determined by Brillouin Light Scattering. *J. Phys. D: Appl. Phys.* **2013**, *46*, 045308.

(10) Si, L. N.; Guo, D.; Luo, J. B.; Lu, X. C. Monoatomic Layer Removal Mechanism in Chemical Mechanical Polishing Process: A Molecular Dynamics Study. *J. Appl. Phys.* **2010**, *107*, 064310.

(11) Han, G. Q.; Liu, Y. H.; Lu, X. C.; Luo, J. B. A Flexible Nanobrush Pad for the Chemical Mechanical Planarization of Cu/Ultra-Low-k Materials. *Nanoscale Res. Lett.* **2012**, *7*, 603.

(12) Liao, C. L.; Guo, D.; Wen, S. Z.; Luo, J. B. Effects of Chemical Additives of CMP Slurry on Surface Mechanical Characteristics and Material Removal of Copper. *Tribol. Lett.* **2012**, *45*, 309−317.

(13) Choi, J. H.; Korach, C. S. Nanoscale Defect Generation in CMP of Low-k/Copper Interconnect Pattern. *J. Electrochem. Soc.* **2009**, *156*, H961−H970.

(14) Gao, M. Z.; Zhang, J. Y.; Wang, Y.; Yu, Z. P. Molecular Dynamics Models of Several Hundreds of Atoms for Back-End-of-Line Dielectrics. *Jpn. J. Appl. Phys.* **2009**, *48*, 04C017.

(15) Takada, S.; Hata, N.; Seino, Y.; Fujii, N.; Kikkawa, T. Dependences of Young's Modulus of Porous Silica Low Dielectric Constant Films on Skeletal Structure and Porosity. *J. Appl. Phys.* **2006**, *100*, 123512.

(16) Urbanowicz, A. M.; Vanstreels, K.; Verdonck, P.; Shamiryan, D.; Gendt, S.; Baklanov, M. R. Improving Mechanical Robustness of Ultralow-k SiOCH Plasma Enhanced Chemical Vapor Deposition Glasses by Controlled Porogen Decomposition Prior to UV-hardening. *J. Appl. Phys.* **2010**, *107*, 104122.

(17) Gourhant, O.; Gerbaud, G.; Zenasni, A.; Favennec, L.; Gonon, P.; Jousseaume, V. Crosslinking of Porous SiOCH films Involving Si−O−C bonds: Impact of Deposition and Curing. *J. Appl. Phys.* **2010**, *108*, 124105.

(18) Karanikas, C. F.; Li, H.; Vlassak, J. J.; Watkins, J. J. Quantitative Interfacial Energy Measurements of Adhesion-Promoted Thin Copper Films by Supercritical Fluid Deposition on Barrier Layers. *J. Eng. Mater. Technol.* **2010**, *132*, 021014.

(19) Iacopi, F.; Travaly, Y.; Eyckens, B.; Waldfried, C.; Abell, T.; Guyer, E. P.; Gage, D. M.; Dauskardt, R. H.; Sajavaara, T.; Houthoofd, K.; Grobet, P.; Jacobs, P.; Maex, K. Short-Ranged Structural Rearrangement and Enhancement of Mechanical Properties of Organosilicate Glasses Induced by Ultraviolet Radiation. *J. Appl. Phys.* **2006**, *99*, 053511.

(20) Dubois, G.; Volksen, W.; Magbitang, T.; Miller, R. D.; Gage, D. M.; Dauskardt, R. H. Molecular Network Reinforcement of Sol−Gel Glasses. *Adv. Mater.* **2007**, *19*, 3989−3994.

(21) Urbanowicz, A. M.; Vanstreels, K.; Verdonck, P.; Besien, E. V.; Christos, T.; Shamiryan, D.; De Gendt, S.; Baklanov, M. R. Effect of UV Wavelength on the Hardening Process of Porogen-Containing and Porogen-Free Ultralow-k Plasma-Enhanced Chemical Vapor Deposition Dielectrics. *J. Vac. Sci. Technol., B: Microelectron. Nanometer Struct.—Process., Meas., Phenom.* **2011**, *29*, 032201.

(22) Urbanowicz, A. M.; Vanstreels, K.; Shamiryan, D.; De Gendt, S.; Baklanov, M. R. Effect of Porogen Residue on Chemical, Optical, and Mechanical Properties of CVD SiCOH Low-k Materials. *Electrochem. Solid-State Lett.* **2009**, *12*, H292−H295.

(23) Urbanowicz, A. M.; Meshman, B.; Schneider, D.; Baklanov, M. R. Stiffening and Hydrophilisation of SOG Low-k Material Studied by Ellipsometric Porosimetry, UV Ellipsometry and Laser-Induced Surface Acoustic Waves. *Phys. Status Solidi A* **2008**, *205*, 829−832.

(24) Thorpe, M. F. Continuous Deformations in Random Networks. *J. Non-Cryst. Solids* **1983**, *57*, 355−370.

(25) Philips, J. C. Topology of Covalent Non-Crystalline Solids I: Short-Range Order in Chalocogenide Alloys. *J. Non-Cryst. Solids* **1979**, *34*, 153−181.

(26) Burkey, D. D.; Gleason, K. K. Structure and Mechanical Properties of Thin Films Deposited from 1, 3, 5-trimethyl-1, 3, 5-trivinylcyclotrisiloxane and Water. *J. Appl. Phys.* **2003**, *93*, 5143−5150.

(27) Tan, C. M.; Li, W.; Gan, C. H. Applications of Finite Element Methods for Reliability Study of ULSI Interconnections. *Microelectron. Reliab.* **2012**, *52*, 1539−1545.

(28) Fukuda, A.; Mochizuki, Y.; Hiyama, H.; Tsujimura, M.; Doi, T.; Kurokawa, S. Stress Analysis of Dielectrics Using FEM for Analyzing

the Cause of Cracking Observed After W-CMP. *J. Electrochem. Soc.* **2009**, *156*, H694−H698.
(29) Liao, C. L.; Guo, D.; Wen, S. Z.; Lu, X. C.; Luo, J. B. Stress Analysis of Cu/Low-k Interconnect Structure during Whole Cu-CMP Process Using Finite Element Method. *Microelectron. Reliab.* **2013**, *53*, 767−773.
(30) Casserly, T. B.; Gleason, K. K. Density Functional Theory Calculation of (29)Si NMR Chemical Shifts of Organosiloxanes. *J. Phys. Chem. B* **2005**, *109*, 13605−13610.
(31) Landers, J.; Yu, G. G.; Neimark, A. V. Density Functional Theory Methods for Characterization of Porous Materials. *Colloids Surf., A* **2013**, *437*, 3−32.
(32) Fan, X. F.; Zheng, W. T.; Chihaia, V.; Shen, Z. X.; Kuo, J. L. Interaction between Graphene and the Surface of SiO_2. *J. Phys.: Condens. Matter.* **2012**, *24*, 305004.
(33) Cuong, N. T.; Otani, M.; Okada, S. Semiconducting Electronic Property of Graphene Adsorbed on (0001) Surfaces of SiO_2. *Phys. Rev. Lett.* **2011**, *106*, 106801.
(34) Tajima, N.; Ohno, T.; Hamada, T.; Yoneda, K.; Kobayashi, N.; Hasaka, S.; Inoue, M. Molecular Modeling of Low-k Films of Carbon-Doped Silicon Oxides for Theoretical Investigations of the Mechanical and Dielectric Properties. *Appl. Phys. Lett.* **2006**, *89*, 061907.
(35) Tajima, N.; Ohno, T.; Hamada, T.; Yoneda, K.; Kondo, S.; Kobayashi, N.; Shinriki, M.; Inaishi, Y.; Miyazawa, K.; Sakota, K.; Hasaka, S.; Inoue, M. Carbon-Doped Silicon Oxide Films with Hydrocarbon Network Bonds for Low-k Dielectrics: Theoretical Investigations. *Jpn. J. Appl. Phys.* **2007**, *46*, 5970.
(36) Yuan, C. A.; Sluis, O.; Zhang, G. Q.; Ernst, L. J.; Driel, W. D.; Flower, A. E.; van Silfhout, R. B. R. Molecular Simulation Strategy for Mechanical Modeling of Amorphous/Porous Low-Dielectric Constant Materials. *Appl. Phys. Lett.* **2008**, *92*, 061909.
(37) Yuan, C. A.; Sluis, O.; Zhang, G. Q.; Ernst, L. J.; Driel, W. D.; Silfhout, R. B. R. Molecular Simulation on the Material/Interfacial Strength of the Low-Dielectric Materials. *Microelectron. Reliab.* **2007**, *47*, 1483−1491.
(38) Li, H.; Knaup, J. M.; Kaxiras, E.; Vlassak, J. J. Stiffening of Organosilicate Glasses by Organic Cross-Linking. *Acta Mater.* **2011**, *59*, 44−52.
(39) Knaup, J. M.; Li, H.; Vlassak, J. J.; Kaxiras, E. Influence of CH_2 Content and Network Defects on the Elastic Properties of Organosilicate Glasses. *Phys. Rev. B* **2011**, *83*, 054204.
(40) Oliver, M. S.; Dubois, G.; Sherwood, M.; Gage, D. M.; Dauskardt, R. H. Molecular Origins of the Mechanical Behavior of Hybrid Glasses. *Adv. Funct. Mater.* **2010**, *20*, 2884−2892.
(41) Sun, H. COMPASS: An ab initio Force-Field Optimized for Condensed-Phase Applications Overview with Details on Alkane and Benzene Compounds. *J. Phys. Chem. B* **1998**, *102*, 7338−7364.
(42) Christensen, M.; Dudiy, S.; Wahnström, G. First-Principles Simulations of Metal-Ceramic Interface Adhesion: Co/WC versus Co/TiC. *Phys. Rev. B* **2002**, *65*, 045408.
(43) Han, Y.; Elliott, J. Molecular Dynamics Simulations of the Elastic Modulus of Polymer/Carbon Nanotube Composites. *Comput. Mater. Sci.* **2007**, *39*, 315−323.
(44) Renner, O.; Zemek, J. Density of Amorphous Silicon Films. *Czech. J. Phys.* **1973**, *23*, 1273−1276.
(45) Adachi, T.; Sakka, S. Dependence of the Elastic Moduli of Porous Silica Gel Prepared by the Sol-Gel Method on Heat-Treatment. *J. Mater. Sci.* **1990**, *25*, 4732−4737.
(46) Ding, Y. F.; Zhang, Y.; Zhang, F. W. Molecular Dynamics Study of the Structure in Vitreous Silica with COMPASS Force Field at Elevated Temperatures. *Mater. Sci. Forum* **2007**, *546−549*, 2189−2193.
(47) Wu, C.; Xu, W. Atomistic Molecular Modelling of Cross-Linked Epoxy Resin. *Polymer* **2006**, *47*, 6004−6009.
(48) Tack, J. L.; Ford, D. M. Thermodynamic and Mechanical Properties of Epoxy Resin DGEBF Crosslinked with DETDA by Molecular Dynamics. *J. Mol. Graphics Modell.* **2008**, *26*, 1269−1275.
(49) Fisher, I.; Kaplan, W. D.; Eizenberg, M. Dielectric Property-Microstructure Relationship for Nanoporous Silica Based Thin Films. *J. Appl. Phys.* **2004**, *95*, 5762.
(50) Si, J. J.; Ono, H.; Uchida, K.; Nozaki, S.; Morisaki, H.; Itoh, N. Correlation between the Dielectric Constant and Porosity of Nanoporous Silica Thin Films Deposited by the Gas Evaporation Technique. *Appl. Phys. Lett.* **2001**, *79*, 3140−3142.
(51) Miyoshi, H.; Matsuo, H.; Oku, Y.; Tanaka, H.; Yamada, K.; Mikami, N.; Takada, S.; Hata, N.; Kikkawa, T. Theoretical Analysis of Elastic Modulus and Dielectric Constant for Low-k Two-Dimensional Periodic Porous Silica Films. *Jpn. J. Appl. Phys.* **2004**, *43*, 498−503.
(52) Heifetsa, E.; Kotomin, E. A. Atomistic Simulation of $SrTiO_3$ and $BaTiO_3$ (110) Surface Relaxations. *Thin Solid Films* **2000**, *358*, 1−5.